Advances in Aircraft and Spacecraft Science, *Vol. 12, No. 1 (2025) 77-93*
https://doi.org/10.12989/aas.2025.12.1.077

Nonlinear resonance and chaos in rotating functionally graded carbon nanotube-reinforced composite annular plates

G.L. She* and J.Q. Xu

College of Mechanical and Vehicle Engineering, Chongqing University, Chongqing 400044, China

(Received February 7, 2025, Revised April 30, 2025, Accepted May 2, 2025)

Abstract. This article investigates the nonlinear forced vibration behavior of a functionally graded carbon nanotube-reinforced composite (FG-CNTRC) rotating annular plate subjected to external excitation forces. First, the governing equations are established based on the first-order shear deformation theory (FSDT) and the Hamiltonian principle. Subsequently, the Galerkin method is utilized to discretize the nonlinear equations. Considering pinned and fixed boundary conditions, the multi-scale method is used to derive analytical solutions. By comparing the results with existing literature, good consistency is achieved, validating the accuracy of the research. Finally, the influences of different parameters on the nonlinear vibration of the annular plate are analyzed. The results indicate that temperature, distribution patterns and volume fraction of CNTs, rotational velocity, and geometric configurations of the plate significantly affect the resonance position. Additionally, the damping coefficient and external load exhibit a pronounced impact on the resonance domain but do not affect the natural frequency. As external excitation varies, periodic motion and chaotic phenomena are observed in the system.

Keywords: annular plate; carbon nanotubes; chaotic phenomena; external excitation; nonlinear forced vibration

1. Introduction

In engineering applications and practical life, plate structures are widely used in numerous fields such as machinery and shipbuilding (Liu *et al.* 2022). The annular plate is a rotating component that has gained increasing attention in practical applications in recent years due to its excellent mechanical performance (Hebali *et al.* 2022). However, under complex working conditions, when the external frequency approaches a critical value, the amplitude of the annular plate increases continuously until it reaches a maximum value, a phenomenon known as resonance. Resonance may cause severe damage to the annular plate structure, leading to economic losses and safety risks. Therefore, studying the resonance behaviors of such structures has significant engineering value (Djilali *et al.* 2022, Abdelrahman *et al.* 2022, Alazwari *et al.* 2022, Melaibari *et al.* 2022a, 2022b).

From existing research, numerous studies by domestic and foreign scholars have focused on free vibration, resonance, chaos, and related phenomena in plate structures. For instance, Valizadeh and Eipakchi (2022) utilized the multi-scale method (MSM) to determine the natural

*Corresponding author, Distinguished Professor, E-mail: sheguilin@cqu.edu.cn

http://www.techno-press.org/?journal=aas&subpage=7 ISSN: 2287-528X (Print), 2287-5271 (Online)

frequency of annular plates under two configurations and explored the amplitude-frequency characteristics. Hu and Xu (2022) analyzed the free vibration of annular plates in a non-uniform magnetic field using MSM. Baferani and Ohadi (2022) investigated the vibrations of annular plates on elastic foundations under various boundary conditions. Ma *et al.* (2022) applied the differential quadrature method (DQM) to study the influence of external loads on chaotic motion in annular plates. Xu *et al.* (2022) derived the second-order approximate analytical expression via MSM to study free vibrations of annular plates under magnetic fields. Using the classical lamination theory, Noroozi and Bakhtiari-Nejad (2021) examined the nonlinear dynamics of trapezoidal plates under primary resonance and 1:3 internal resonance conditions. Guo *et al.* (2023) combined the first-order shear deformation theory (FSDT) and Rayleigh-Ritz method to analyze vibrational behaviors and obtain amplitude-frequency response curves for laminated plates considering 1:1 internal resonance. Zhou *et al.* (2021) integrated experimental and numerical approaches to study the forced vibration response of plates. Li *et al.* (2023) investigated nonlinear resonance and chaos in rotating circular plates in two distinct environments using MSM. Zhang and Chen (2021) examined chaotic behavior in simply supported plates under dual excitations via a global perturbation method. In recent years, composite materials have advanced significantly, among which functionally graded carbon nanotube-reinforced composites (FG-CNTRC) have been widely adopted in plates, shells, and beams due to their superior strength and stiffness (Huang *et al.* 2022, Cuong-Le *et al.* 2019). For example, Thanh *et al.* (2017) employed the Airy stress function to analyze the nonlinear dynamic response of FG-CNTRC plates under temperature and load variations. Dat *et al.* (2022) applied the fourth-order Runge-Kutta method to study the effects of loads and CNT parameters on the dynamic response of FG-CNTRC plates. Shen *et al.* (2019) developed a weak-form orthogonal element method to investigate geometric nonlinear dynamics in FG-CNTRC rectangular plates under explosive loading. More relevant works can refer to (Assie 2024, Dastjerdi *et al.* 2021a, 2021b, 2023a, 2023c, Cai and She 2025, Fan and She 2025, Fan *et al.* 2025, Gan and She 2025a, 2025b, Li and She 2025a, 2025b, She and He 2025, She *et al.* 2025a, 2025b, Xu *et al.* 2025).

Although extensive research has been conducted on free vibration and nonlinear resonance of annular plates, existing literature reveals a gap in studying resonance of FG-CNTRC annular plates under external excitation. To address this, the present article focuses on the primary resonance of FG-CNTRC annular plates. The results demonstrate that temperature, CNT distribution patterns, volume fraction, rotational speed, and geometric dimensions significantly influence the resonance position. Furthermore, damping and external forces modify the resonance domain but do not affect the natural frequency. As the external force varies, periodic motion and chaotic phenomena can be observed in the system.

2. Mathematical modelling

The model structure used in this paper is displayed in Fig. 1. For ease of description, a cylindrical coordinate system (r, θ, z) is established with the center of the annular plate as the origin. The z-axis aligns with the thickness direction of the annular plate, which has a thickness of h, an inner radius of R_b, an outer radius of R_a, and rotates at a speed R_t. The top surface of the plate is subjected to an external load $F(t)$. The annular plate material is a composite composed of carbon nanotubes (CNTs) and an isotropic matrix. Fig. 2 illustrates the three CNT distribution patterns: UD, FG-V, and FG-O. To account for the effective physical properties of the composite material,

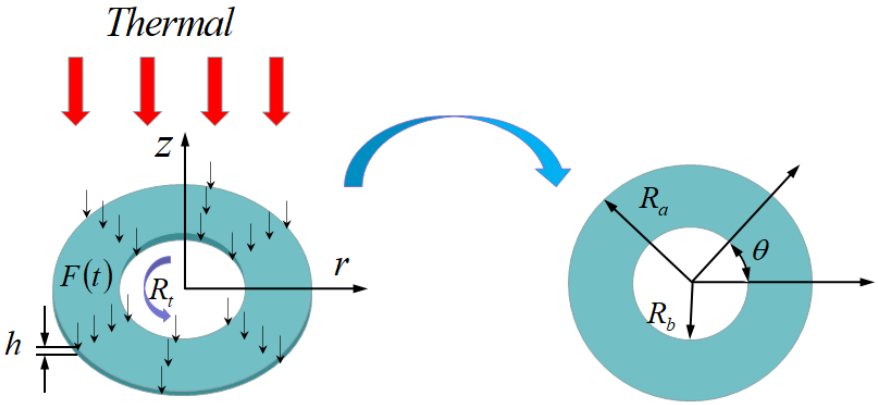

Fig. 1 Configuration of an FG-CNTRC plate

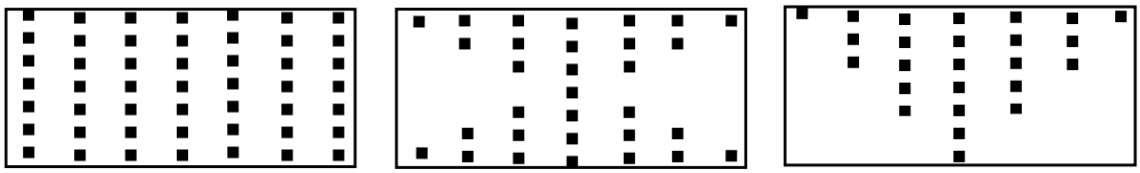

(a) UD (b) FG-X (c) FG-V

Fig. 2 Schematic diagram of CNTs distribution patterns (Modified from Babaei 2022)

the article introduces efficiency parameters $\eta_i (i=1,2,3)$, which characterize the material properties as referenced in prior studies (Babaei *et al.* 2022).

$$E_{11} = \eta_1 V_{cnt} E_{11}^{cnt} + (1 - V_{cnt}) E^p \tag{1}$$

$$\frac{\eta_2}{E_{22}} = \frac{V_{cnt}}{E_{22}^{cnt}} + \frac{(1-V_{cnt})}{E^p} \tag{2}$$

$$\frac{\eta_3}{G_{12}} = \frac{V_{cnt}}{G_{12}^{cnt}} + \frac{(1-V_{cnt})}{G^p} \tag{3}$$

$$v = V_{cnt} v^{cnt} + (1 - V_{cnt}) v^p \tag{4}$$

$$\rho = V_{cnt} \rho^{cnt} + (1 - V_{cnt}) \rho^p \tag{5}$$

$$\alpha_{11} = \frac{E^p \alpha^p (1-V_{cnt}) + E_{11}^{cnt} \alpha_{11}^{cnt} V_{cnt}}{E^p (1-V_{cnt}) + E_{11}^{cnt} V_{cnt}} \tag{6}$$

$$\alpha_{22} = (1 + v_{12}^{cnt}) V_{cnt} \alpha_{22}^{cnt} + (1 + v^p)(1 - V_{cnt}) \alpha^p - v \alpha_{11} \tag{7}$$

The above equations describe the equivalent material properties of FG-CNTRC, where CNT denotes the carbon nanotube material parameters, and p represents the polymer matrix parameters. Here, E_{11} and E_{22} are the elastic moduli in the axial and transverse directions, G_{12} is the shear modulus, v is Poisson's ratio, and ρ is the density. The subscripts 11 and 22 correspond to the axial and transverse directions of the CNTs, respectively. V_{CNT} represents the volume fraction of CNTs, and the material parameter definitions follow Babaei (2022)

$$\begin{aligned} &\text{UD:} V_{\text{cnt}} = V_{\text{cnt}}^{*} \\ &\text{FG-X:} V_{\text{cnt}} = 2\left(1 - 2\frac{|z|}{h}\right) V_{\text{cnt}}^{*} \\ &\text{FG-V:} V_{\text{cnt}} = V_{\text{cnt}}^{*}\left(1 + 2\frac{z}{h}\right) \end{aligned} \tag{8}$$

in which

$$V_{\text{cnt}}^{*} = \frac{W_{cnt}}{W_{cnt} + (\rho^{cnt} + \rho^{m})(1 - W_{cnt})} \tag{9}$$

Unless otherwise specified, the matrix material characterizations in this paper are as follows (Babaei 2022)

$$\begin{aligned} &E^{p} = (3.52 - 0.0034T)\text{GPa}, \\ &\alpha^{p} = 45(1 + 0.0005\Delta T)10^{-6}/\text{K}, \\ &v^{p} = 0.34. \end{aligned} \tag{10}$$

In the above expressions, $\Delta T = T - 300K$, and the related material parameters in Eqs. (1)-(7) are defined as follows

$$\begin{aligned} &E_{11}^{cnt}(T)(\text{TPa}) = -4.458333 \times 10^{-9}T^{3} + 7.43 \times 10^{-6}T^{2} - 4.338417 \times 10^{-3}T + 6.3998, \\ &E_{22}^{cnt}(T)(\text{TPa}) = -5.5625 \times 10^{-9}T^{3} + 9.275 \times 10^{-6}T^{2} - 5.420375 \times 10^{-3}T + 8.02155, \\ &G_{12}^{cnt}(T)(\text{TPa}) = 4.479167 \times 10^{-9}T^{3} - 6.965 \times 10^{-6}T^{2} + 3.476208 \times 10^{-3}T + 1.40755, \\ &\alpha_{11}^{cnt}(T)(10^{-6}/K) = 1.13625 \times 10^{-8}T^{3} - 2.887 \times 10^{-5}T^{2} + 0.02291688T - 1.12515, \\ &\alpha_{22}^{cnt}(T)(10^{-6}/K) = 1.25 \times 10^{-11}T^{3} + 2.9 \times 10^{-7}T^{2} - 0.984625 \times 10^{-4}T + 5.43715, \\ &v_{12}^{cnt} = 0.175. \end{aligned} \tag{11}$$

3. Governing equations

This paper focuses on two deformation modes in the vibration of rotating annular plates: symmetric and asymmetric deformation. Based on the first-order shear deformation theory (FSDT), the displacement field is formulated as follows (Zhang *et al*. 2023, Yang *et al*. 2023)

$$\begin{aligned} &u_{r}(r,\theta,z,t) = u(r,\theta,t) + z\phi_{r}(r,\theta,t), \\ &u_{\theta}(r,\theta,z,t) = v(r,\theta,t) + z\phi_{\theta}(r,\theta,t), \\ &u_{z}(r,\theta,z,t) = w(x,\theta,t). \end{aligned} \tag{12}$$

In this context, the cylindrical coordinates *r*, θ, and time *t* define the displacement components of the plate. Within the displacement field representation, *u*, *v*, *w* represent the mid-plane displacements along the *r*, θ, and *z* directions, respectively, while ψ_r and ψ_θ denote the rotational components of the cross-section. Following the nonlinear von Kármán theory, the strain field is expressed as

$$\begin{aligned} \varepsilon_{rr} &= u_{rr} + \frac{1}{2}u_{zr}^{2}, \\ \varepsilon_{\theta\theta} &= \frac{1}{r}u_{r} + \frac{1}{r}u_{\theta,\theta} + \frac{1}{2r^{2}}u_{z,\theta}^{2}, \\ \gamma_{r\theta} &= \frac{1}{r}u_{r,\theta} + u_{\theta,r} - \frac{1}{r}u_{\theta} + \frac{1}{r}u_{z,\theta}u_{z,r}, \\ \gamma_{rz} &= u_{r,z} + u_{z,r}, \\ \gamma_{z\theta} &= \frac{1}{r}u_{z,\theta} + u_{\theta,z}. \end{aligned} \tag{13}$$

The constitutive relationship of annular plates can be described as

$$\begin{bmatrix}\sigma_{rr}\\ \sigma_{\theta\theta}\\ \tau_{rz}\\ \tau_{r\theta}\\ \tau_{z\theta}\end{bmatrix}=\begin{bmatrix}Q_{11} & Q_{12} & 0 & 0 & 0\\ Q_{12} & Q_{22} & 0 & 0 & 0\\ 0 & 0 & Q_{55} & 0 & 0\\ 0 & 0 & 0 & Q_{44} & 0\\ 0 & 0 & 0 & 0 & Q_{66}\end{bmatrix}\cdot\left(\begin{bmatrix}\varepsilon_{rr}\\ \varepsilon_{\theta\theta}\\ \gamma_{rz}\\ \gamma_{r\theta}\\ \gamma_{z\theta}\end{bmatrix}-\begin{bmatrix}\alpha\\ \alpha\\ 0\\ 0\\ 0\end{bmatrix}\Delta T\right) \tag{14}$$

Herein, the stiffness coefficient can be refer to Zhang *et al.* (2023).

This paper applies Hamiltonian principle to derive the control equations for the rotating FG-CNTRC annular plates

$$\int_t\left(\delta T-\delta U-\delta U_R+\delta W_F+\delta W_{qf}\right)dt=0 \tag{15}$$

The definition for the kinetic energy T, strain energy U, and potential energy U_R of the annular plate are as follows (Yang *et al.* 2023)

$$\begin{aligned}T&=\int_{R_b}^{R_a}\int_0^{2\pi}\int_{-\frac{h}{2}}^{\frac{h}{2}}\frac{1}{2}\rho_{(z)}\begin{bmatrix}(\dot{u}_r-\Omega u_\theta)^2\\ +\left(\dot{u}_\theta+\Omega(r+u_r)\right)^2+\dot{u}_z^2\end{bmatrix}r\,dz\,d\theta dr\\ U&=\frac{1}{2}\int_{R_b}^{R_a}\int_0^{2\pi}\int_{-\frac{h}{2}}^{\frac{h}{2}}\begin{pmatrix}\sigma_{rr}\varepsilon_{rr}+\sigma_{\theta\theta}\varepsilon_{\theta\theta}+\tau_{r\theta}\gamma_{r\theta}\\ +K_s\tau_{z\theta}\gamma_{z\theta}\end{pmatrix}+K_s\tau_{rz}\gamma_{rz})r\,dz\,d\theta dr\\ U_R&=\int_{R_b}^{R_a}\int_0^{2\pi}\int_{-\frac{h}{2}}^{\frac{h}{2}}-\rho r\Omega^2u_r r\,dz\,d\theta dr\end{aligned} \tag{16}$$

The work done by the load and damping can be expressed as

$$\begin{aligned}W_F&=\int_{R_b}^{R_a}\int_0^{2\pi}-F(t)u_z r\,d\theta dr\\ W_{qf}&=\int_{R_b}^{R_a}\int_0^{2\pi}q_f\,u_z\,rd\theta dr\end{aligned} \tag{17}$$

wherein

$$\begin{aligned}q_f(r,\theta,t)&=-C_t\frac{\partial w}{\partial t},K_s=\pi^2/12\\ F(t)&=\mathbb{Q}\cos\omega t\end{aligned} \tag{18}$$

In which, $\mathbb{Q}$ stands for the amplitude of external load and ω indicates frequency, substituting Eqs. (12)-(14) and (16)-(17) into Eq. (15) results in the nonlinear control equations (Yang *et al.* 2023, Zhang *et al.* 2023)

$$\frac{\partial N_{rr}}{\partial r}+\frac{1}{r}\frac{\partial N_{r\theta}}{\partial\theta}+\frac{1}{r}(N_{rr}-N_{\theta\theta})+I_0r\Omega^2=I_0\frac{\partial^2u_0}{\partial t^2}+I_1\frac{\partial^2\varphi_r}{\partial t^2}-2I_0\Omega\frac{\partial v_0}{\partial t}-2I_1\Omega\frac{\partial\varphi_\theta}{\partial t}, \tag{19}$$

$$\frac{\partial N_{r\theta}}{\partial r}+\frac{1}{r}\frac{\partial N_{\theta\theta}}{\partial\theta}+\frac{2}{r}N_{r\theta}=I_0\frac{\partial^2v_0}{\partial t^2}+I_1\frac{\partial^2\varphi_\theta}{\partial t^2}+2I_0\Omega\frac{\partial u_0}{\partial t}+2I_1\Omega\frac{\partial\varphi_r}{\partial t}, \tag{20}$$

$$\begin{aligned}&\frac{\partial Q_{rr}}{\partial r}+\frac{1}{r}\frac{\partial Q_{\theta\theta}}{\partial\theta}+\frac{Q_{rr}}{r}+\frac{\partial N_{rr}}{\partial r}\frac{\partial w_0}{\partial r}+N_{rr}\frac{\partial^2w_0}{\partial r^2}-N_{rr}^T\frac{\partial^2w_0}{\partial r^2}+\frac{N_{\theta\theta}}{r^2}\frac{\partial^2w_0}{\partial\theta^2}-\frac{N_{\theta\theta}^T}{r^2}\frac{\partial^2w_0}{\partial\theta^2}+\frac{2N_{r\theta}}{r}\frac{\partial^2w_0}{\partial r\,\partial\theta}+\\ &\frac{1}{r}\frac{\partial N_{r\theta}}{\partial r}\frac{\partial w_0}{\partial\theta}+\frac{N_{rr}}{r}\frac{\partial w_0}{\partial r}-k_ww_0+\frac{k_g}{r}\frac{\partial w_0}{\partial r}+\frac{1}{r^2}\frac{\partial N_{\theta\theta}}{\partial\theta}\frac{\partial w_0}{\partial\theta}+\frac{1}{r}\frac{\partial N_{r\theta}}{\partial\theta}\frac{\partial w_0}{\partial r}+k_g\frac{\partial^2w_0}{\partial r^2}+\frac{k_g}{r^2}\frac{\partial^2w_0}{\partial\theta^2}-\\ &c_t\frac{\partial w_0}{\partial t}+p(t)=I_0\left(\frac{\partial^2w_0}{\partial t^2}-\Omega^2\frac{\partial^2w_0}{\partial\theta^2}\right),\end{aligned} \tag{21}$$

$$\frac{\partial M_{rr}}{\partial r}+\frac{1}{r}\frac{\partial M_{r\theta}}{\partial \theta}+\frac{1}{r}(M_{rr}-M_{\theta\theta})-Q_{rr}+I_1 r\Omega^2=I_1\frac{\partial^2 u_0}{\partial t^2}+I_2\frac{\partial^2 \varphi_r}{\partial t^2}-2I_1\Omega\frac{\partial v_0}{\partial t}-2I_2\Omega\frac{\partial \varphi_\theta}{\partial t}, \quad (22)$$

$$\frac{\partial M_{r\theta}}{\partial r}+\frac{1}{r}\frac{\partial M_{\theta\theta}}{\partial \theta}+\frac{2}{r}M_{r\theta}-Q_{\theta\theta}=I_1\frac{\partial^2 v_0}{\partial t^2}+I_2\frac{\partial^2 \varphi_\theta}{\partial t^2}+2I_1\Omega\frac{\partial u_0}{\partial t}+2I_2\Omega\frac{\partial \varphi_r}{\partial t}. \quad (23)$$

in which

$$\begin{gathered}\left(A_{ij},B_{ij},D_{ij}\right)=\int_{-\frac{h}{2}}^{\frac{h}{2}}(1,z,z^2)\,Q_{11}dz,(ij=11,22,44,55,66),\\ [I_0,I_1,I_2]=\int_{-\frac{h}{2}}^{\frac{h}{2}}\rho(z)[1,z,z^2]\,dz\end{gathered} \quad (24)$$

4. Solution method

In this section, the boundary conditions incorporating all four edges simply supported are considered for the rotating annular plate. The Galerkin method is used to discretize the governing equations; simultaneously, a multiscale analysis is employed to obtain the global solution.

$$[u,\phi_r]=\sum_{m=1}^{\infty}\sum_{n=1}^{\infty}[U(t),\Psi_X(t)]\frac{\partial X_m(r)}{\partial r}Y_n(r), \quad (25)$$

$$[u,\phi_r]=\sum_{m=1}^{\infty}\sum_{n=1}^{\infty}[U(t),\Psi_X(t)]\frac{\partial X_m(r)}{\partial r}Y_n(r), \quad (26)$$

$$w=\sum_{m=1}^{\infty}\sum_{n=1}^{\infty}W(t)X_m(r)Y_n(\theta). \quad (27)$$

In this formulation, $U(t)$, $V(t)$, $W(t)$, $\varphi_x(t)$, $\varphi_y(t)$ the generalized coordinates of displacements in the mid-plane and rotational degrees of freedom. Given the simply supported boundary conditions, the modal function $X(r)$ can be expressed in the form

$$X(r)=sin(\frac{r-R_b}{R_a-R_b}),Y(\theta)=sin(\theta) \quad (28)$$

By substituting Eqs. (25)-(27) into Eqs. (19)-(23) and applying the Galerkin method, we derive the governing equations (Zhang *et al.* 2023)

$$I_0\frac{d^2W(t)}{dt^2}+C_t\frac{dW(t)}{dt}+F_1W(t)+F_2[W(t)]^2+F_3[W(t)]^3=F\,cos(\Omega t) \quad (29)$$

In addition, Eq. (29) can be analyzed via the multiple-scale method; following the solution procedure outlined in Gan and She (2025a), we derive the approximate solution.

5. Numerical analyses

The next step is to verify the validity of the proposed method. As shown in Table 1, the natural frequencies of the annular plate (geometric parameters: h=0.1 m, R_a=2 m, R_b=0.5 m) are compared with existing references. The current results demonstrate excellent agreement with those reported by Wu *et al.* (2019) and Tornabene *et al.* (2009), thereby confirming the accuracy of the model.

Table 2 lists the dimensionless natural frequencies for vibration modes with different

Table 1 Comparison of natural frequencies for isotropic homogeneous annular plates (h=0.1 m, R_a=2 m, R_b=0.5 m, m=n=1)

Source	Present	Wu *et al.* (2019)	Tornabene *et al.* (2009)
Natural frequency	114.02	115.4174	115.417

Table 2 Dimensionless natural frequencies under different modes (h=0.04 m, R_a=3 m, R_b=2 m, C_d=1000, C_t=1000, ΔT=100, *UD*, V_{cnt}*=0.12, R_t=0.1, F=1 MPa, $\Phi = \Omega\sqrt{(R_a/A_{11m}/h)}$)

m	Dimensionless natural frequencies Φ				
	n=1	n=2	n=3	n=4	n=5
1	0.7803	0.7944	0.8392	0.9136	1.0098
2	1.6906	1.6976	1.7196	1.7578	1.8103
3	2.5800	2.5847	2.5994	2.6248	2.6604

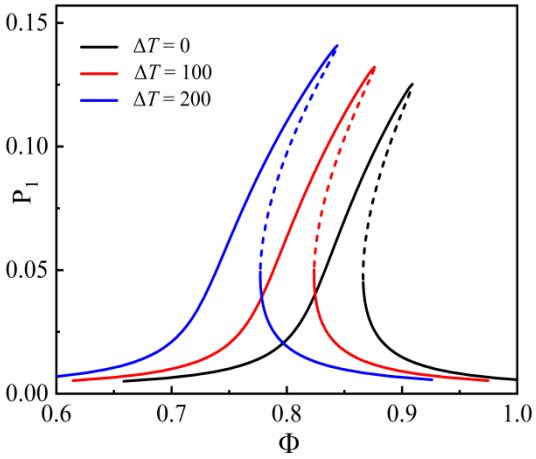

Fig. 3 Effect of temperature (h=0.04 m, R_a=3 m, R_b=2 m, C_t=2000, *UD*, V_{cnt*}=0.12, R_t =0.1, F=1 MPa, ε=0.01)

wavenumber combinations. Based on these results, the fundamental mode (m=1, n=1) is selected for subsequent analysis.

Fig. 3 reveals the effect of temperature changes on the dynamic response of the forced oscillation. The results show that the resonance position of the FG-CNTRC annular plates shifts with temperature under simply supported boundary conditions. This phenomenon is attributed to the temperature-dependent material properties. As the temperature increases, the resonance probability rises, and the peak amplitude of the resonance curve becomes larger. Therefore, lowering the temperature not only improves the fundamental frequency of the annular plates, delaying resonance onset, but also reduces the maximum radial deformation.

Fig. 4 depicts the influence of rotational speed. With the rotational speed increasing from 0 to 0.2, significant changes occur in both the resonance position and maximum deflection. Specifically, increasing the rotational speed enhances the natural frequency, delays resonance, and reduces the vibration amplitude peak. These observations indicate that rotational speed effectively enhances the structural stiffness and improves the vibration resistance of the plates.

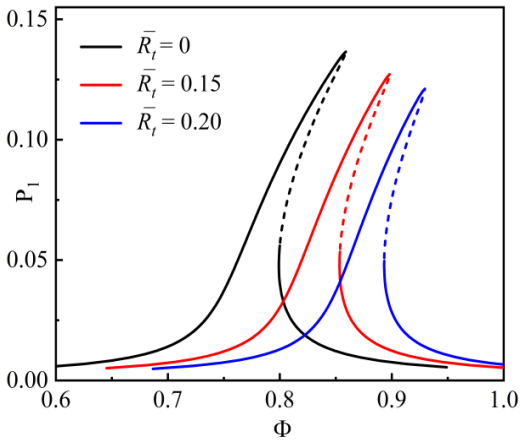

Fig. 4 Effect of rotating speed (h=0.04 m, R_a=3 m, R_b=2 m, C_t=2000, ΔT=100, *UD*, V_{cnt^*}=0.12, F=1 MPa, ε=0.01)

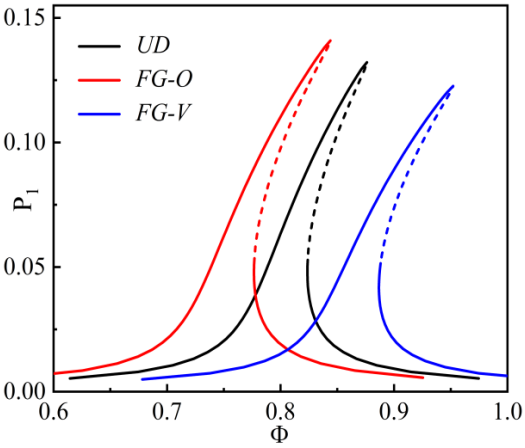

Fig. 5 Effect of distribution mode of CNTs (h=0.04 m, R_a=3 m, R_b=2 m, C_t=2000, ΔT=100, V_{cnt^*}=0.12, R_t=0.1, F=1 MPa, ε=0.01)

Fig. 5 displays the effect of CNT distribution patterns (UD, FG-O, FG-V) on the forced oscillation response. The FG-V distribution yields the highest fundamental frequency, followed by UD and FG-O. However, the maximum radial deformation trend is reversed: FG-O exhibits the largest deflection, while FG-V shows the smallest. This discrepancy arises because the FG-V pattern significantly improves the elastic modulus, thereby enhancing stiffness.

Fig. 6 analyzes the impact of CNT volume fraction in UD mode (ΔT=100 K, F=1 MPa). Increasing the CNT volume fraction shifts the resonance curve rightward and significantly reduces the vibration amplitude peak, demonstrating that higher CNT content strengthens oscillation resistance.

Fig. 7 illustrates the effect of the damping coefficient. Increased damping reduces the maximum deflection, whereas decreased damping amplifies the amplitude peak and broadens the resonance domain. Notably, the damping coefficient does not alter the resonance position despite its influence on dynamic deflection.

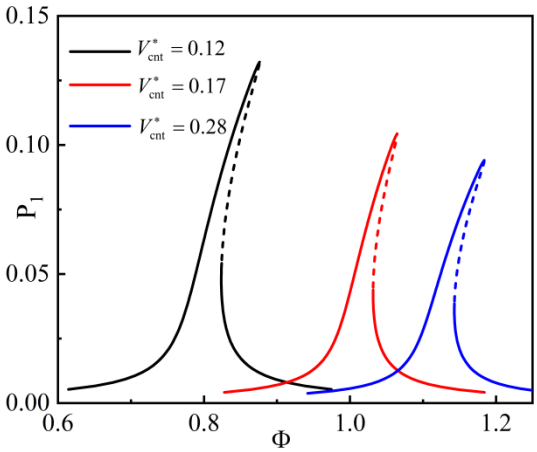

Fig. 6 Effect of CNTs volume fraction (h=0.04 m, R_a=3 m, R_b=2 m, C_t=2000, ΔT=100, *UD*, R_t=0.1, F=1 MPa, ε=0.01)

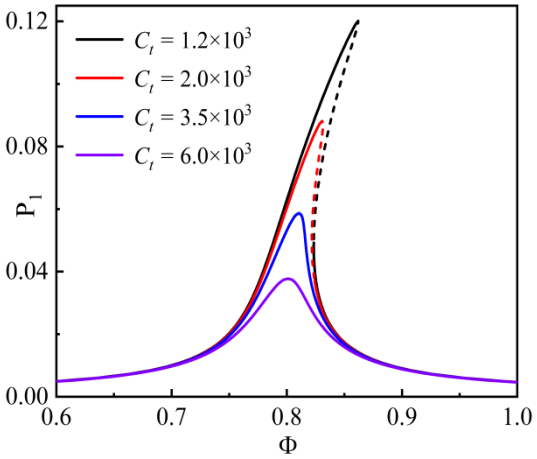

Fig. 7 Effect of damping coefficient (h=0.04 m, R_a=3 m, R_b=2 m, ΔT=100, *UD*, V_{cnt*}=0.12, R_t=0.1, F=1 MPa, ε=0.01)

Fig. 8 indicates the effect of R_b/h ratio on dynamic response. A larger R_b/h ratio accelerates resonance onset and increases vibration amplitude. Fig. 9 further examines the radius ratio (R_a/R_b). As R_a/R_b increases, the natural frequency decreases, and resonance occurs earlier—a trend consistent with Fig. 8. These findings confirm that smaller R_a/R_b ratios enhance vibration resistance.

Fig. 10 illustrates the effect of external loads. The excitation force does not shift the resonance position (i.e., it preserves the natural frequency) but significantly amplifies the radial deflection and expands the resonance region with increasing load magnitude.

Fig. 11 focuses on the dynamic behavior of the system under external excitation at C_t =1000. The results reveal that the system exhibits periodic-to-chaotic transitions under varying excitation forces. Four representative cases (Points A-D) are analyzed:

• At Point A, the system displays single-period motion.

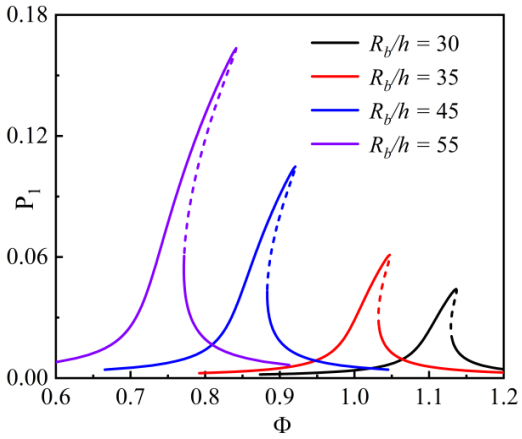

Fig. 8 Effect of R_b/h (h=0.04 m, R_a=3 m, C_t=2000, ΔT=100, *UD*, V_{cnt*}=0.12, R_t=0.1, F=1 MPa, ε=0.01)

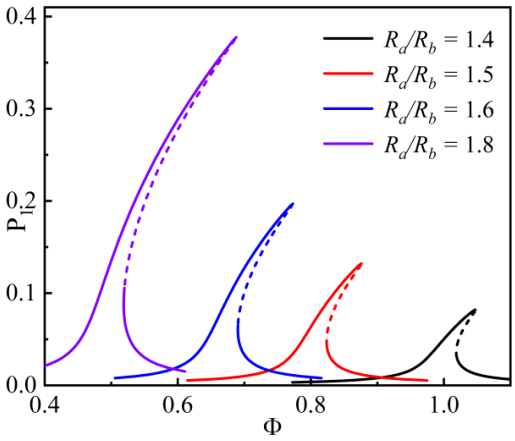

Fig. 9 Effect of R_a/R_b (h=0.04 m, R_b=3 m, *S-S*, C_t=2000, ΔT=100, *UD*, V_{cnt*}=0.12, R_t=0.1, F=1 MPa, ε=0.01)

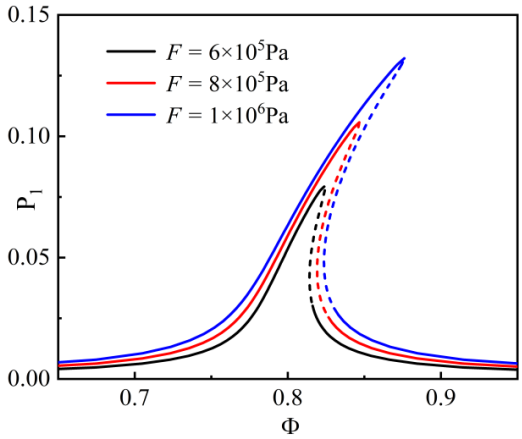

Fig. 10 Effect of F (h=0.04 m, R_a=3 m, R_b=2 m, *S-S*, C_t=2000, ΔT=100, *UD*, V_{cnt*}=0.12, R_t=0.1, ε=0.01)

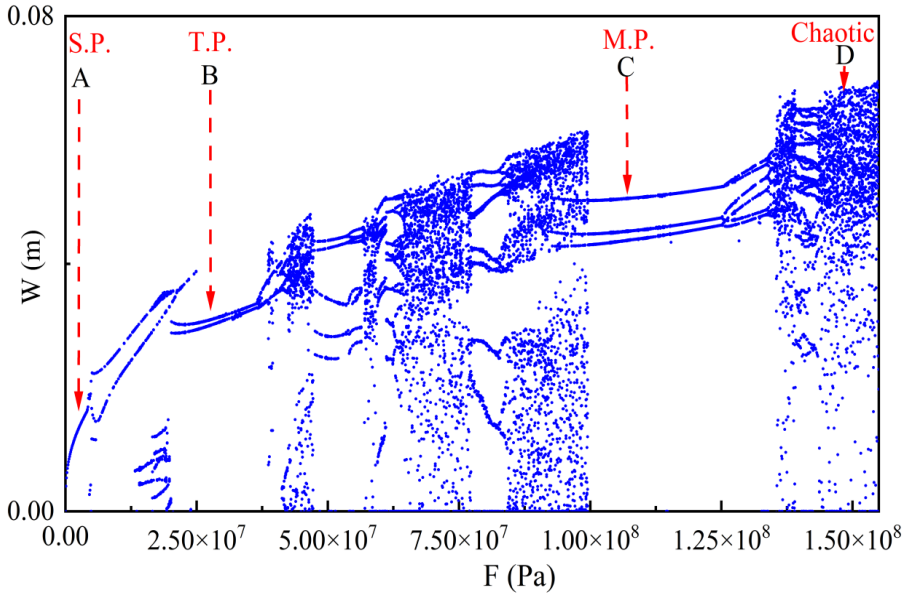

Fig. 11 Maximum amplitude changes with external excitation (h=0.04 m, R_a=3 m, R_b=2 m, C_t=10000, *UD*, V_{cnt*}=0.12, R_t=0.1, ε=0.01)

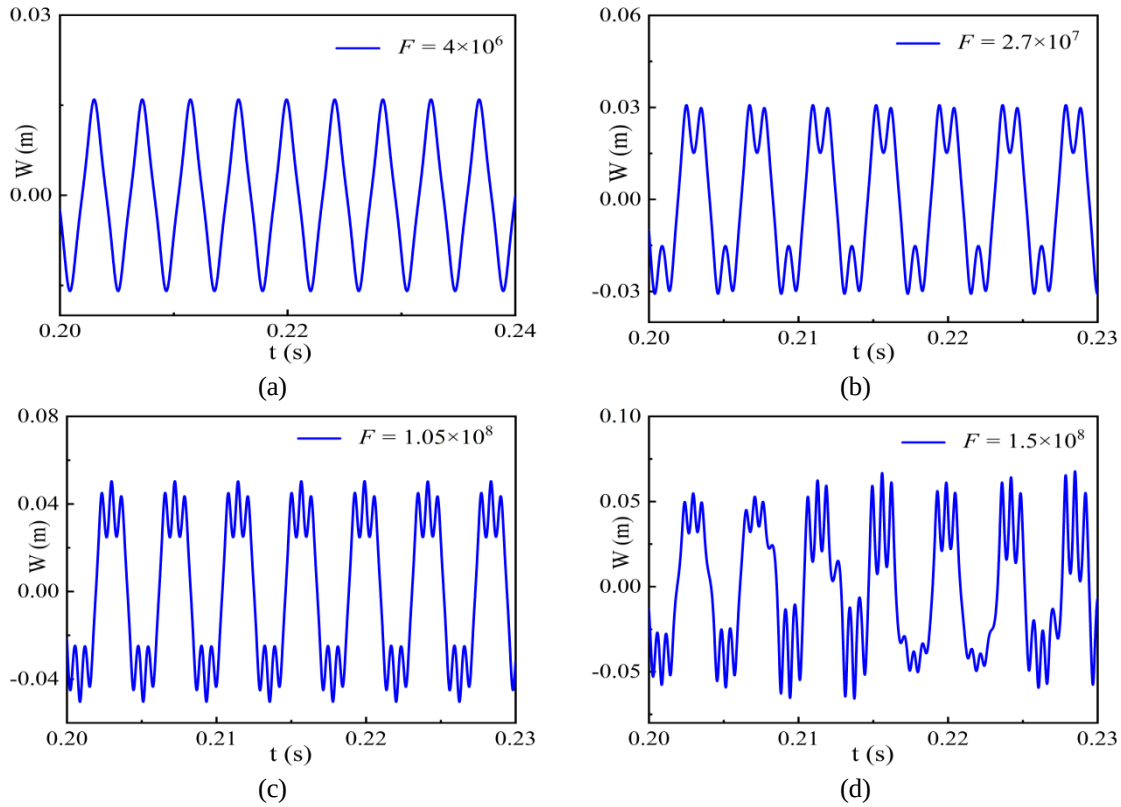

Fig. 12 Time history image (h=0.04 m, R_a=3 m, R_b=2 m, *S-S*, C_t=1000, *UD*, V_{cnt*}=0.12, R_t=0.1, F=1 MPa, ε=0.01)

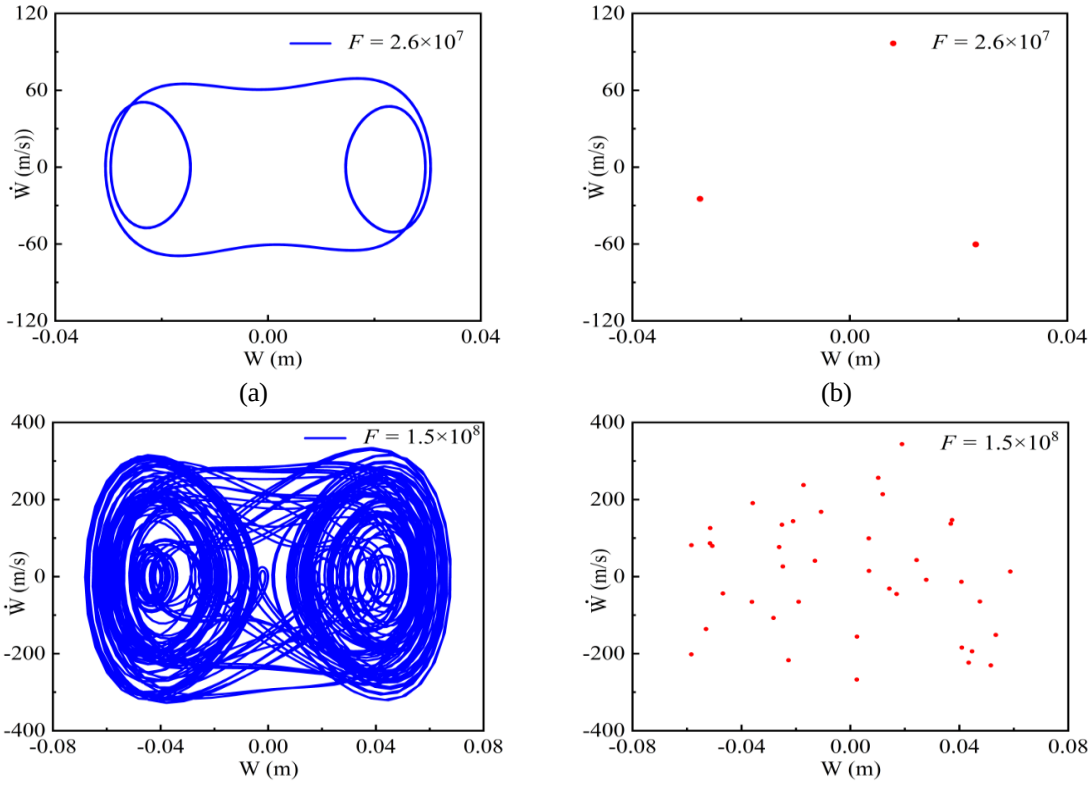

Fig. 13 Phase diagram (h=0.04 m, R_a=3 m, R_b=2 m, C_t=1000, *UD*, V_{cnt*}=0.12, R_t=0.1, F=1 MPa, ε=0.01)

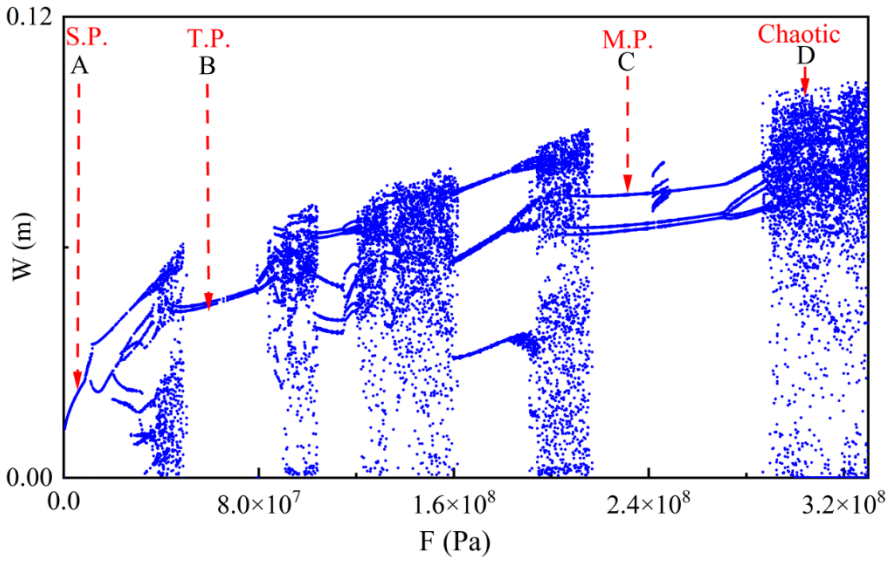

Fig. 14 Maximum amplitude changes with external excitation (h=0.04 m, R_a=3 m, R_b=2 m, C_t=8000, *UD*, V_{cnt*}=0.12, R_t=0.1, ε=0.01)

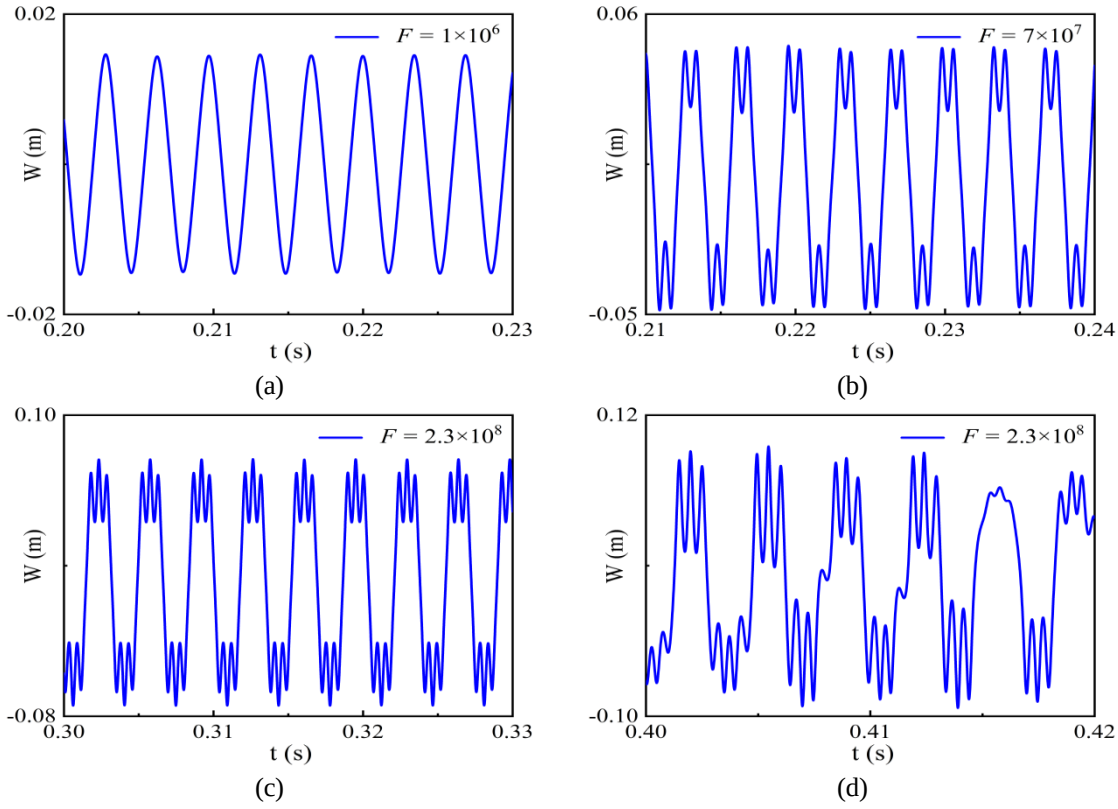

Fig. 15 Time history image (h=0.04 m, R_a=3 m, R_b=2 m, C_t=8000, *UD*, V_{cnt*}=0.12, R_t=0.1, F=1 MPa, ε=0.01)

- At Point B, period-doubling bifurcation occurs.
- At Point C, three-period quasiperiodic motion emerges.
- At Point D (F=1.5×10^8 Pa), the system transitions to fully developed chaos, as evidenced by the time-history plots (Fig. 12 (c), (d)) and phase portraits (Fig. 13 (c), (d)).

Notably, increasing the excitation force (2.5×10^7 Pa<F<1.0×10^8 Pa) amplifies the vibration amplitude, as confirmed by both time-history (Fig. 12) and phase diagrams (Fig. 13). Similar phenomena are observed in Figs. 14-16, which depict the bifurcation diagram, time-history response, and phase trajectories at Ct=800.

6. Conclusions

This study investigates the nonlinear forced vibration of rotating functionally graded carbon nanotube-reinforced composite (FG-CNTRC) annular plates under external loads. Two boundary conditions (simply supported and clamped) are considered, with a focus on resonance behavior influenced by multiple factors: temperature, rotational speed, CNT distribution patterns, volume fraction of CNTs, damping coefficient, geometric parameters (radius ratio R_a/R_b, thickness h), and external excitation amplitude. Key conclusions are summarized as follows:

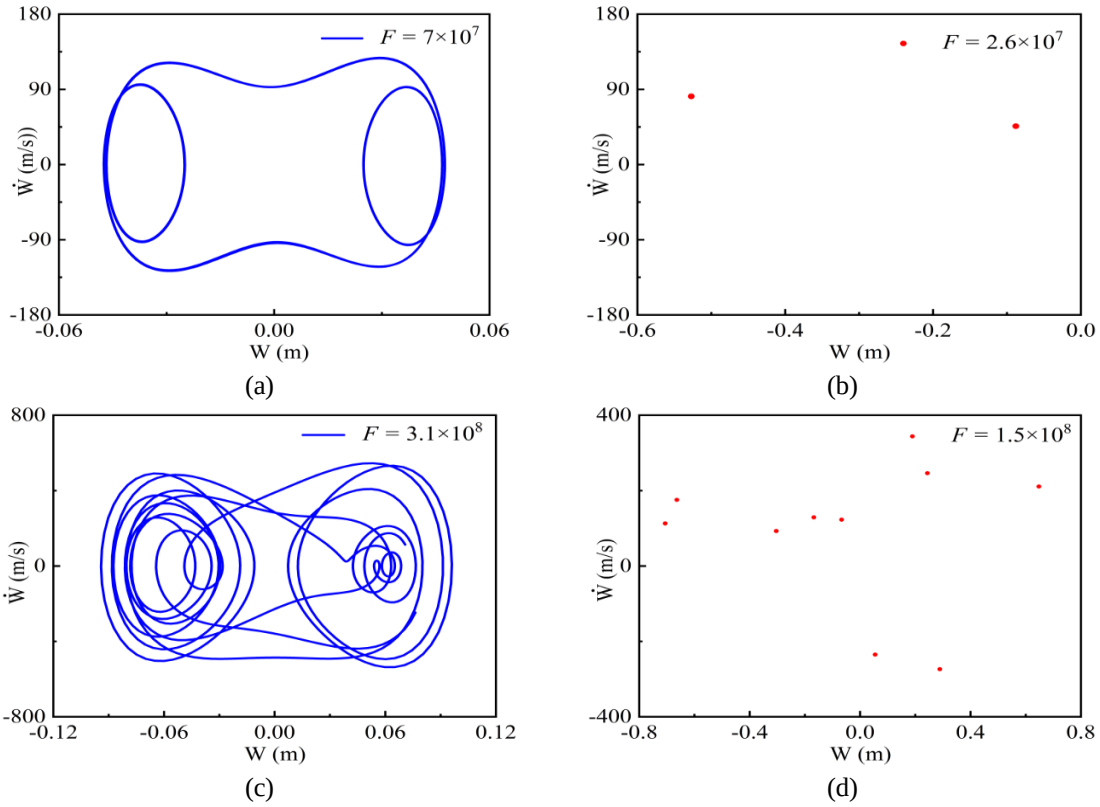

Fig. 16 Phase diagram (h=0.04 m, R_a=3 m, R_b=2 m, C_t=8000, *UD*, V_{cnt*}=0.12, R_t=0.1, F=1 MPa, ε=0.01)

1. Temperature rise shifts the resonance position forward and reduces the maximum radial deflection.
2. Increased rotational speed elevates the natural frequency, thereby suppressing resonance occurrence.
3. CNT reinforcement significantly enhances the mechanical properties of the plates. FG-V distribution exhibits superior vibration resistance compared to UD and FG-O patterns.
4. Geometric parameters (e.g., R_a/R_b, h) critically affect resonance characteristics, with smaller *Ra*/*Rb* ratios improving vibration resistance.
5. Damping coefficient and excitation amplitude do not alter the resonance frequency, but lower damping or higher excitation forces amplify peak radial deformation and broaden the resonance bandwidth.
6. The system exhibits rich dynamic transitions, including periodic, quasiperiodic, and chaotic motions, under varying excitation forces.

References

Abdelrahman, A.A., Shanab, R.A., Esen, I. and Eltaher, M.A. (2022), "Effect of moving load on dynamics of nanoscale Timoshenko CNTs embedded in elastic media based on doublet mechanics theory", *Steel*

Compos. Struct., **44**(2), 241-256. https://doi.org/10.12989/scs.2022.44.2.241.
Alazwari, M.A., Daikh, A.A. and Eltaher, M.A. (2022), "Novel quasi 3D theory for mechanical responses of FG-CNTs reinforced composite nanoplates", *Adv. Nano. Res*., **12**(2), 117-137. https://doi.org/10.12989/anr.2022.12.2.117.
Assie, A.E. (2024), "Nonlinear bending analysis of bidirectional graded porous plates with elastic foundations relative to neutral surface", *Adv. Aircraft Spacecraft Sci.*, **11**(2), 129-152. https://doi.org/10.12989/aas.2024.11.2.129.
Babaei, H. (2022), "Thermomechanical analysis of snap-buckling phenomenon in long FG-CNTRC cylindrical panels resting on nonlinear elastic foundation", *Compos. Struct*., **286**, 115199. https://doi.org/10.1016/j.compstruct.2022.115199.
Baferani, A.H. and Ohadi, A.R. (2022), "Effect of in-plane loads on the natural frequencies of transversely isotropic thick annular sector plates resting on elastic foundation", *Proc. Inst. Mech. Eng. Part C-J. Mech. Eng. Sci*., **236**(14), 8057-8072. https://doi.org/10.1177/09544062221084191.
Cai, Y. and She, G.L. (2025), "Nonlinear dynamic response of magneto-electro-elastic cylindrical shells subjected to moving load", *Mech. Adv. Mater. Struct.*, 1-12. https://doi.org/10.1080/15376494.2025.2463090.
Cuong-Le, Thanh., Tran, L.V., Vu-Huu, T., Nguyen-Xuan, H. and Abdel-Wahab, M. (2019), "Size-dependent nonlinear analysis and damping responses of FG-CNTRC micro-plates", *Comput. Meth. Appl. Mech. Eng.*, **353**, 253-276. https://doi.org/10.1016/j.cma.2019.05.002.
Dastjerdi, S., Alibakhshi, A., Akgoz, B. and Civalek, O. (2023a), "On a comprehensive analysis for mechanical problems of spherical structures", *Int. J. Eng. Sci.*, **183**, 103796. https://doi.org/10.1016/j.ijengsci.2022.103796.
Dastjerdi, S., Civalek, O., Malikan, M. and Akgoz, B. (2023b), "On analysis of nanocomposite conical structures", *Int. J. Eng. Sci.*, **191**, 103918. https://doi.org/10.1016/j.ijengsci.2023.103918.
Dastjerdi, S., Malikan, M., Eremeyev, V.A., Akgoz, B. and Civalek, O. (2021a), "On the generalized model of shell structures with functional cross-sections", *Compos. Struct.*, **272**, 114192. https://doi.org/10.1016/j.compstruct.2021.114192.
Dastjerdi, S., Naeijian, F., Akgoz, B. and Civalek, O. (2021b), "On the mechanical analysis of microcrystalline cellulose sheets", *Int. J. Eng. Sci.*, **166**, 103500. https://doi.org/10.1016/j.ijengsci.2021.103500.
Dat, N.D., Thanh, N.V., MinhAnh, V. and Duc, N.D. (2022), "Vibration and nonlinear dynamic analysis of sandwich FG-CNTRC plate with porous core layer", *Mech. Adv. Mater. Struct.*, **29**(10), 1431-1448. https://doi.org/10.1080/15376494.2020.1822476.
Djilali, N., Bousahla, A.A., Kaci, A., Selim, M.M., Bourada, F., Tounsi, A., Tounsi, A., Benrahou, K.H. and Mahmoud, S.R. (2022), "Large cylindrical deflection analysis of FG carbon nanotube-reinforced plates in thermal environment using a simple integral HSDT", *Steel Compos. Struct*., **42**(6), 779-789. https://doi.org/10.12989/scs.2022.42.6.779.
Fan, Y.H. and She, G.L. (2025) "Nonlinear transient response of graphene platelets reinforced metal foams beam considering initial geometrical imperfection and viscoelastic elastic foundation", *Comput. Concrete*, **35**(1), 59-70. https://doi.org/10.12989/cac.2025.35.1.059.
Fan, Y.H., She, G.L. and Li, C. (2025), "Nonlinear transient response analysis of revolution doubly curved shells", *Arch. Civil Mech. Eng.*, **25**, 145. https://doi.org/10.1007/s43452-025-01187-6.
Foroutan, K. and Dai, L. (2024). "Nonlinear free and forced vibrations of oblique stiffened porous FG shallow shells embedded in a nonlinear elastic foundation", *Struct. Eng. Mech.*, **89**(1), 33-46. https://doi.org/10.12989/sem.2024.89.1.033.
Gan, L.L. and She, G.L. (2025a), "Nonlinear combined resonance of magneto-electro-elastic plates", *Eur. J. Mech.-A/Solid.*, **109**, 105492. https://doi.org/10.1016/j.euromechsol.2024.105492.
Gan, L.L. and She, G.L. (2025b), "Nonlinear transient responses of FG-CNTRC cylindrical shells: Influence of hygro-thermal effect", *Comput. Concrete*, **35**(5), 557-567. https://doi.org/10.12989/cac.2025.35.5.557.
Guo, X.Y., Zhang, Y.M., Luo, Z. and Cao, D.X. (2023), "Nonlinear dynamics analysis of a graphene laminated composite plate based on an extended Rayleigh-Ritz method", *Thin Wall. Struct.*, **186**, 110673.

https://doi.org/10.1016/j.tws.2023.110673.
Hebali, H., Chikh, A., Bousahla, A.A., Bourada, F., Tounsi, A., Benrahou, K.H., Hussain, M. and Tounsi, A. (2022), "Effect of the variable visco-Pasternak foundations on the bending and dynamic behaviors of FG plates using integral HSDT model", *Geomech. Eng.*, **28**(1), 49-64. https://doi.org/10.12989/gae.2022.28.1.049.
Hu, Y.D. and Xu, H.R. (2022), "Nonaxisymmetric magnetoelastic coupling natural vibration analysis of annular plates in an induced nonuniform magnetic field", *Nonlin. Dyn.*, **109**(2), 657-687. https://doi.org/10.1007/s11071-022-07475-7.
Huang, X.H., Yang, J., Wang, X.E. and Azim, I. (2022), "Combined analytical and numerical approach for auxetic FG-CNTRC plate subjected to a sudden load", *Eng. Comput.*, **38**, 55-70. https://doi.org/10.1007/s00366-020-01106-8.
Li, W.Q., Hu, Y.D. and Li, Z. (2023), "Magneto-aero-elastic superharmonic and subharmonic resonances, bifurcations and chaos of conductive spinning circular plates", *Int. J. Bifurc. Chaos*, **33**(01), 2330001. https://doi.org/10.1142/S021812742330001X.
Li, Y.P. and She, G.L. (2025a), "Nonlinear dynamic response of porous graphene platelets reinforced plates subjected to moving load considering initial geometrical imperfection", *J. Vib. Eng. Technol.*, **13**(1), 17. https://doi.org/10.1007/s42417-024-01651-2.
Li, Y.P. and She, G.L. (2025b), "Nonlinear dynamic response of graphene platelets reinforced cylindrical shells under moving loads considering initial geometric imperfection", *Eng. Struct.*, **323**(A), 119241. https://doi.org/10.1016/j.engstruct.2024.119241.
Liu, Z.F., Wu, X.Y., Yu, M. and Habibi, M. (2022), "Large-amplitude dynamical behavior of multilayer graphene platelets reinforced nanocomposite annular plate under thermo-mechanical loadings", *Mech. Bas. Des. Struct. Mach.*, **50**(11), 3722-3746. https://doi.org/10.1080/15397734.2020.1815544.
Ma, L.H., Liu, X.L. and Moradi, Z. (2022), "On the chaotic behavior of graphene-reinforced annular systems under harmonic excitation", *Eng. Comput.*, **38**(3), 2583-2607. https://doi.org/10.1007/s00366-020-01210-9.
Melaibari, A., Daikh, A.A., Basha, M., Abdalla, A.W., Othman, R., Almitani, K.H., Hamed, M.A., Abdelrahman, A. and Eltaher, M.A. (2022a), "Free vibration of FG-CNTRCs nano-plates/shells with temperature-dependent properties", *Math.*, **10**(4), 583. https://doi.org/10.3390/math10040583,2022.
Melaibari, A., Daikh, A.A., Basha, M., Wagih, A., Othman, R., Almitani, K.H., Hamed, M.A., Abdelrahman, A. and Eltaher, M.A. (2022b), "A dynamic analysis of randomly oriented functionally graded carbon nanotubes/fiber-reinforced composite laminated shells with different geometries", *Math.*, **10**(3), 408. https://doi.org/10.3390/math10030408.
Noroozi, M. and Bakhtiari-Nejad, F. (2021), "Nonlinear vibration of a nanocomposite laminated piezoelectric trapezoidal actuator in subsonic airflow under combined electrical and forcing excitations", *Proc. Inst. Mech. Eng. Part C-J. Mech. Eng.*, **235**(2), 4784-4817. https://doi.org/10.1177/0954406220911075.
She, G.L. and He, Y.J. (2025), "Nonlinear thermal buckling of magneto-electro-thermal-elastic plates with geometric imperfection", *Struct. Eng. Mech.*, **93**(2), 115-123. https://doi.org/10.12989/sem.2025.93.2.115.
She, G.L., Gan, L.L. and Xu, J.Q. (2025a), "Nonlinear snap-buckling of graphene platelet reinforced metal foams doubly curved shells with geometric imperfection", *Geomech. Eng.*, **40**(3), 183-191. https://doi.org/10.12989/gae.2025.40.3.183.
She, G.L., Ma, Z.S., Li, C. and Eltaher, M.A. (2025b), "Geometrically nonlinear transient response of graphene platelets reinforced metal foams arbitrary quadrilateral plates under blast load", *Thin Wall. Struct.*, **210**, 113018. https://doi.org/10.1016/j.tws.2025.113018.
Shen, Z.Q., Xia, J. and Cheng, P. (2019), "Geometrically nonlinear dynamic analysis of FG-CNTRC plates subjected to blast loads using the weak form quadrature element method", *Compos. Struct.*, **209**, 775-788. https://doi.org/10.1016/j.compstruct.2018.11.009.
Thanh, N.V., Khoa, N.D., Tuan, N.D., Tran, P. and Duc, N.D. (2017), "Nonlinear dynamic response and vibration of functionally graded carbon nanotube-reinforced composite (FG-CNTRC) shear deformable plates with temperature-dependent material properties and surrounded on elastic foundations", *J. Therm.*

Stress., **40**(10), 1254-1274. https://doi.org/10.1080/01495739.2017.1338928.
Tornabene, F., Viola, E. and Inman, D.J. (2009), "2-D differential quadrature solution for vibration analysis of functionally graded conical, cylindrical shell and annular plate structures", *J. Sound Vib.*, **328**(3), 259-290. https://doi.org/10.1016/j.jsv.2009.07.031.
Valizadeh, R. and Eipakchi, H. (2022), "Effect of transverse and radial deformations on nonlinear frequencies of annular plates: Perturbation approach", *Ship. Offsh. Struct.*, **17**(9), 2058-2069. https://doi.org/10.1080/17445302.2021.1979720.
Wu, H.L., Zhu, J., Kitipornchai, S., Wang, Q., Ke, L.L. and Yang J. (2020), "Large amplitude vibration of functionally graded graphene nanocomposite annular plates in thermal environments", *Compos. Struct.*, **239**, 112047. https://doi.org/10.1016/j.compstruct.2020.112047.
Xu, H.R., Hu, Y.D. and Hao, Y. (2022), "Magnetoelastic nonlinear free vibration of an annular plate under a nonuniform magnetic field of the long straight current-carrying wire", *Zamm-Zeitschrift Fur Angewandte Mathematik Und Mechanik*, **102**(6), e202000299. https://doi.org/10.1002/zamm.202000299.
Xu, J.Q., Li, Y.P. and She, G.L. (2025), "Nonlinear low-velocity impact response of GPLRMF doubly curved shells in thermal environment", *Comput. Concrete*, **35**(3), 219-229. https://doi.org/10.12989/cac.2025.35.3.219.
Yang, Y., Li, J., Chen, B., Dong, Y. and Li, Y. (2023), "Symmetric and asymmetric vibrations of rotating GPLRC annular plate", *Int. J. Mech. Sci.*, **250**, 108282. https://doi.org/10.1016/j.ijmecsci.2023.108282.
Zhai, Y.C., Yu, X., Yue, X.J., Wang, P.H. and Zhang, P. (2021), "Dynamic property of functionally graded carbon nanotube-reinforced composite plates with viscoelastic core", *Compos. Struct*., **275**, 114466. https://doi.org/10.1016/j.compstruct.2021.114466.
Zhang, Y.W., She, G.L. and Eltaher, M.A. (2023), "Nonlinear transient response of graphene platelets reinforced metal foams annular plate considering rotating motion and initial geometric imperfection", *Aerosp. Sci. Technol.*, **142**, 108693. https://doi.org/10.1016/j.ast.2023.108693.
Zhou, Z.W., Chen, M.X., Xiong, Y.P., Jia, W.C., Dong, W.K. and Xie, K. (2021), "Experimental and mixed analytical-numerical studies for free and forced vibrations of Z-reinforced sandwich plates stiffened by steel ribs", *Compos. Struct*., **272**, 114221. https://doi.org/10.1016/j.compstruct.2021.114221.

CC